ACS APPLIED MATERIALS & INTERFACES

Research Article

Cite This: ACS Appl. Mater. Interfaces XXXX, XXX, XXX−XXX

www.acsami.org

# Thin Biobased Transparent UV-Blocking Coating Enabled by Nanoparticle Self-Assembly

Emily Olson,[†,§] Yifan Li,[†] Fang-Yi Lin,[‡] Ana Miller,[†] Fei Liu,[†] Ayuna Tsyrenova,[†] Devin Palm,[†] Greg W. Curtzwiler,[§] Keith L. Vorst,[§] Eric Cochran,[‡] and Shan Jiang*[,†,§,∥]

[†]Department of Materials Science & Engineering, [‡]Department of Chemical & Biological Engineering, and [§]Polymer and Food Protection Consortium and Department of Food Science and Human Nutrition, Iowa State University, Ames, Iowa 50011, United States

[∥]Division of Materials Science & Engineering, Ames National Laboratory, Ames, Iowa 50011, United States

Supporting Information

**ABSTRACT:** A waterborne, UV-blocking, and visually transparent nanocomposite coating was formulated with ZnO nanoparticles and 2-hydroxyethyl cellulose (HEC). The coating is highly effective (<5% UV and ∼65% visible transmittance), and the film thickness (0.2−2.5 μm) is ∼100 times thinner than the conventional coatings of similar UV-blocking performance. The superior properties are due to the fractal structures of ZnO nanoparticles assembled within the HEC matrix, revealed by scanning electron microscopy and small-angle X-ray scattering (SAXS). Changing the binder to 2-hydroxyethyl starch (HES) diminishes the UV-blocking performance, as ZnO nanoparticles form dense globular aggregates, with an aggregation number measured by SAXS 3 orders of magnitude larger than the HEC coating. Since HEC and HES share the same repeating glucose unit in the polymer backbone, it suggests that the conformational characteristics of the binder polymer have a strong influence on the nanoparticle aggregation, which plays a key role in determining the optical performance. Similar structures were achieved with $TiO_2$ nanoparticles. This study not only offers a cost-effective and readily scalable method to fabricate transparent UV-blocking coating but also demonstrates that the unique fractal aggregation structures in a nanocomposite material can provide high performance and functionality without fully dispersing the nanoparticles.

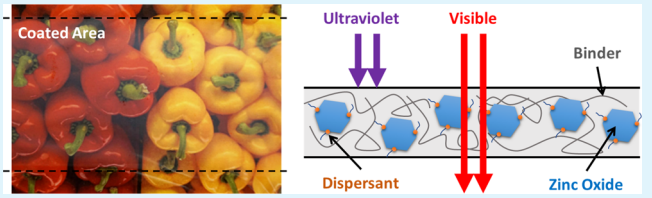


**KEYWORDS:** *UV-blocking, biobased coatings, waterborne coatings, hydroxyethyl cellulose, ZnO nanoparticles*



## INTRODUCTION

Ultraviolet (UV) protection is critical to human skin health and material preservation. There are three types of UV radiation: UVA (320−400 nm), UVB (290−320 nm), and UVC (290−100 nm). Though UVC is absorbed by the atmosphere, UVA and UVB radiation reach the earth at 95 and 5% of the total UV radiation, respectively.[1] Generally, excessive exposure to sunlight induces the degradation of organic materials, loss of mechanical strength, and pigment fading. Therefore, various industries have a great level of interest in protective coatings with UV-blocking capability to prevent photodegradation.[2] The same principle can be extended to food protection. It has been found that UV exposure has significant impacts on discoloration and flavor defects.[3] In meat packaging, UV protection can help prevent fresh meats from experiencing myoglobin oxidation, resulting in the color fade.[4] There is also significant interest in utilizing UV protection for plastic bottles to maintain the taste of dairy or prevent vitamin degradation of sports drinks or juices.[5] In addition, lipid-rich snacks undergo oxidative rancidity in transparent bags, and increased UV protection could slow this process and increase shelf life.[6] From cosmetics to food packaging, oftentimes UV protection and optical transparency are both desirable. Therefore, significant efforts have been invested in developing transparent UV-blocking systems using both organic UV-blocking agents and inorganic nanoparticles.

The most widely studied inorganic nanoparticles are ZnO and $TiO_2$ due to their inherent absorbing and scattering properties.[7] The optical properties of these particles within coating films are highly dependent on nanoparticle size, distribution, and refractive index.[8] In addition, these nanoparticles have received a great amount of attention within the scientific community and industry for their electrical, optical, catalytic, antibacterial, and thermal properties.[9−18] It is generally believed that nanoparticle dispersity is critical to the functionality of nanocomposites, including the UV-blocking capability.[19,20] Therefore, the aggregation of nanoparticles may significantly reduce UV-blocking efficiency and functionality. For example, $TiO_2$ nanoparticles, which trade at multi-billion-dollar market volumes, are most commonly applied in coating formulations as an opacifier due to the high reflective index. Improving the efficiency of $TiO_2$

Received: March 27, 2019
Accepted: June 17, 2019
Published: June 17, 2019




DOI: 10.1021/acsami.9b05383
ACS Appl. Mater. Interfaces XXXX, XXX, XXX−XXX

nanoparticles is a critical challenge in the coating industry as the nanoparticles tend to aggregate and lose their scattering efficiency when coatings dry.[21] To thoroughly disperse nanoparticles, their concentration is usually kept dilute, or the nanoparticle surface is chemically conjugated with charged groups or polymers to prevent aggregation.[22] For example, an oil-based emulsion surface was utilized to modify ZnO nanoparticles and create a transparent, hydrophobic UV absorbent coating to protect the color and integrity of textiles.[23] ZnO nanoparticles can also be surface modified with aminopropyl trimethoxy silane for nanoparticle dispersity in aqueous suspension and reinforcement in phthalonitrile composites.[24] Similarly, ZnO nanoparticles can be capped with carboxymethyl cellulose for dispersion in starch matrices as a means of improving hydrophobicity and antimicrobial activity in food packaging.[25] Highly dispersed ZnO nanoparticles have also been shown in polyvinyl butyral matrices as a glass coating.[26] In addition, different polymers have been tested as matrices to disperse ZnO nanoparticles, including polyurethane, epoxy, and acrylate systems. All these studies hinge on the proposition that dispersing ZnO nanoparticles is essential for nanocomposite to be transparent and block UV radiation efficiently. One way to prevent aggregation is to build a thick coating film to space out the nanoparticles. For this reason, the typical coating thickness reported for an effective UV-blocking coating using ZnO nanoparticles is usually larger than 50 $\mu$m.[27−31] However, for many applications, thinner films are often desired for economic or functional considerations, such as less material consumption, better flexibility, improved adhesion, and better crack resistance.

In this paper, we show that high UV-blocking efficacy can be achieved through control of the ZnO nanoparticle aggregation without full ZnO dispersion. Furthermore, we demonstrate that the choice of the binder has a profound impact on the formation of hierarchically self-assembled structures of nanoparticles in a thin coating film. Two widely used biobased polymer derivatives were studied here: 2-hydroxyethyl starch (HES) and 2-hydroxyethyl cellulose (HEC).[32,33] Our results indicate that the delicate conformational differences in the polymer binders can lead to dramatic differences in the nanoparticle aggregation patterns and UV-blocking performance of the thin films. Our discovery is significant for the fabrication of nanocomposites that require high nanoparticle concentration. This is especially relevant for applications within constrained space, such as a thin layer of the coating film, where aggregations can hardly be avoided.

The study presented here indicates that it is critical to consider the influence of the polymer binder morphology on nanoparticle aggregation when designing a nanocomposite material. In addition, different types of nanoparticles show similar assembly structures when formulated with HEC and HES binders, which suggests that the unique structures may not be specific to nanoparticle surface chemistry. There may be a universal mechanism that drives the self-assembly of nanoparticles using the systems described in this work. This study offers alternative approaches to disperse nanoparticles in the polymer matrix and may inspire the creation of new nanocomposite materials for more broad applications.

## RESULTS AND DISCUSSION

**Coating Formulation and UV-Blocking Performance.** Our coating formulation has three key elements: UV-blocking agent, polymeric binder, and chemical dispersant. A variety of commercial ZnO nanoparticles were tested as UV-blocking agents, including predispersed ZnO nanoparticles (∼15 nm) (Figure S1) and nanopowders (∼50 nm). The unique band gap of hexagonal wurtzite ZnO promotes UV-blocking in the UVA range, which has been proven to be the most vital portion of the spectrum in the promotion of food degradation.[34] There are two major reasons to choose ZnO nanoparticles. First, under the same volume, nanoparticles have a much larger surface area compared with micron size particles, which will enhance the UV-blocking efficiency. Second, nanoparticles are much smaller than the wavelength of the visible light, so that the scattering of visible light is minimized, and the nanocomposite can maintain the transparency.

This study tested biobased starch and cellulose polymer derivatives: HES and HEC. The molecular weight of the polymeric binder was also investigated, as it can affect rheology and UV-blocking capabilities of the coating film. Two molecular weights of HEC were analyzed: a high molecular weight of 1 300 000 g/mol (1.3 M) and a significantly lower molecular weight of 90 000 g/mol (90k). It was found that the larger molecular weight of HEC (1.3 M) became significantly more viscous at comparable loading levels of its lower molecular weight counterpart (90k). To match the coating drawdown thicknesses, the loading levels of different molecular weights of HEC were adjusted to equate the viscosities at ∼65 cP under a shear rate of 50 rpm. With these parameters in mind, the 1.3 M HEC concentration was set at 0.5 wt %, whereas the dosing of 90k HEC is set at 4 wt %. The UV performance and visible transparency are comparable for both formulations (Figure S2). However, the reduced polymer content in the high-molecular-weight solution yields a much thinner and concentrated film for 1.3 M HEC. Additionally, the higher level of steric repulsion in 1.3 M HEC offers a means of stability against sedimentation in the coating formulation for an extended time.

When the coating film dries, limited space inevitably crowds nanoparticles and induces aggregation. The aggregation has two effects: (1) the nanoparticle surface available for absorbing UV radiation is decreased; (2) large aggregates scatter more visible light and deteriorate the transparency. Hence, a small amount of chemical dispersant was added to prevent the formation of large aggregates. The sodium polyphosphate dispersant was used for ZnO and $TiO_2$ nanopowders. For the ZnO nanoparticle dispersion, since the nanoparticle surface was already modified with silane and dispersible in water, a small amount of Tween 20 (0.5 wt %) was added to help further improve the dispersion of ZnO nanoparticles in the solution. However, dispersant alone cannot fully determine the aggregation of ZnO nanoparticles and achieve the high UV-blocking efficacy. The critical component of the coating formulation is the polymeric binder. Figure 1 compares the UV-blocking performance of coating formulated with HEC and HES with ZnO. The UV performance of the same coatings with $TiO_2$ is shown in the Supporting Information (Figure S3). At a similar level of nanoparticle concentration and viscosity, HEC formulation shows excellent UV-blocking capability (>90% blocking), whereas HES does not block UV effectively (∼ 10% blocking). The results are rather surprising since HEC and HES share almost the same chemical composition in the polymer backbone. The only difference is the bond orientation of the repeating glucose unit (trans vs cis).

**Thin Thickness.** Thin coatings have several advantages such as less material consumption, better flexibility, improved


DOI: 10.1021/acsami.9b05383
ACS Appl. Mater. Interfaces XXXX, XXX, XXX−XXX

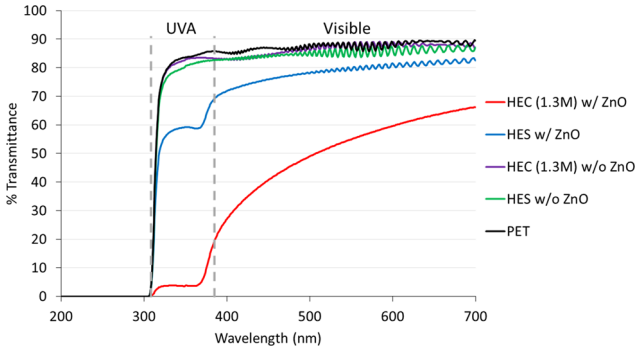


**Figure 1.** Comparison of UV−vis spectrum for poly(ethylene terephthalate) (PET) substrate alone, PET substrate coated with HEC (1.3 M), HES, HEC (1.3 M) with ZnO, and HES with ZnO coatings. When combined with ZnO, HEC greatly outperforms HES in terms of coating efficacy.

adhesion, and crack resistance. However, attaining thin and UV-blocking films proves a difficult task, as lengthy measures are often required to disperse ZnO nanoparticles within the matrix. To accurately measure the film thickness, we carefully examined the coating film cross-section under a confocal laser microscope (Figure S4) and a high-resolution scanning electron microscope (SEM) (Figure S5). Herein, our coating has a thickness (0.2−2.5 $\mu$m) that is much lower than that of conventional technologies (>50 $\mu$m) with comparable UV-blocking performance. Though limited volume in thin coatings is known to cause random nanoparticle aggregation and diminished optical performance, in this study, HEC is found to retain UV-blocking performance in thin coatings. Imaging at nanoscale revealed that this unique property is due to the formation of fractal nanoparticle assembly structures.

Table 1 briefly summarizes some of the results from previous studies side-by-side with the results in our study. It is evident that our coating is much thinner, and the use of ZnO nanoparticles is among the most efficient, considering the amount of added ZnO and thickness of the coating film.

**Table 1. Comparison of UV-Blocking Films Formulated Using ZnO Nanoparticles**

| | | | transmittance | |
|---|---|---|---|---|
| binder choice | ZnO content in formulation[a] | thickness [$\mu$m] | UVA [354 nm] | visible [600 nm] |
| this study: HEC | 0.8% | 0.2−2.5 | 5% | 65% |
| polyacrylate[27] | 2% | 40 | 8% | 80% |
| acrylic emulsion[28] | 2% | 45 | 15% | 57% |
| starch + keferin[29] | 1% | 130 | 2%[b] | 79%[b] |
| polylactide[30] | 1% | 140 | 6%[b] | 79%[b] |
| polyurethane/ acrylic[31] | 2% | 2000 | 7% | 85% |

[a]Nanoparticle content is estimated in the wet coating formulation due to the variation among coating composition and thickness when dried. [b]Values of transmittance are calculated from extrapolated absorbance values.

**Polymeric Binder.** When formulated with HEC and ZnO nanoparticles, the final coating film demonstrated high transparency at the visible wavelength range (~65%) and UV-blocking efficiency (~95%), as shown in Figure 1 and Table 1. Interestingly, when loaded with the same amount of ZnO nanoparticles in HES, the coating film lost almost all of the UV-blocking capabilities. Since HEC and HES have almost identical chemical compositions in the polymer backbone, the results are rather unexpected. One possible explanation is linked to the differences in the conformations of HEC and HES molecules. In starch, the glucose units are connected through a cis ($\alpha$) glycosidic bond, whereas in cellulose, the bond is trans ($\beta$). The difference in bond orientation drastically changes the conformation and morphology of the polymer chains in the aqueous solution. A previous study has shown in aqueous solutions, HEC molecules indeed behave as rigid and extended chains, whereas for the aqueous solutions of amylose (precursor of HES), dynamic light scattering measurements and calculations indicate that the polymers cannot have extended helical, rodlike structures.[32,33] Here, persistence length, $l_p$, can be used to characterize the polymer chain stiffness; when $l_p$ is comparable to or greater than the contour length, the polymer will behave as stiff rigid rods. For values of $l_p$ much smaller than the contour length, the chains are flexible and adopt random coil-like conformations. Prior studies of modified starch and its derivatives indicate that HES has a significantly shorter persistence length of ~6 nm, compared to HEC whose persistence length is ~40 nm.[32,33] Thus, HES adopts a more coil-like conformation, whereas HEC adopts a more extended rodlike conformation in the aqueous solutions. The compact structure of HES in the aqueous solution also limits its capability to thicken the formulation. Therefore, HEC is a much more efficient thickener than HES of similar molecular weight.

To understand the dramatic UV-blocking performance between HEC and HES, the details of ZnO nanoparticle aggregations were examined under SEM (Figure 2). HEC and HES coating films showed completely different ZnO aggregation structures. In Figure 2b, when HES was used as the binder polymer, ZnO nanoparticles aggregated into separated, dense clusters. These kinds of aggregates have been often observed for nanocomposite materials.[35−37] However, in Figure 2a, when HEC was used as the polymeric binder, ZnO nanoparticles formed intriguing fractal network structures with significant open space within the network. A similar phenomenon has been observed with ZnO in colloidal suspensions.[38] The structures showed great resemblance to the branched structures formed by diffusion-limited aggregation, which suggests that strong attractions may exist among nanoparticles and induce aggregation upon contact when the coating films dry. Since all of the other conditions for these two coating formulations were kept the same, it is apparent that different ZnO nanoparticle aggregation structures are due to the morphology differences between HEC and HES.

The comparison between HEC and HES suggests that the molecular architecture of the polymer backbone has profound effects upon the particle aggregation within the nanocomposite. We hypothesize that the extended rodlike structures of HEC may induce strong attractions among ZnO nanoparticles during the drying process of the coating film. Two possible mechanisms should be considered. The first consideration is bridging: when volume shrinks as the coating film dries, rodlike HEC chains may form bridges among ZnO nanoparticles, bringing the particles together. Since HEC has an extended conformation with high persistence length, the bridging may happen more efficiently and at a much longer distance than with HES. A second consideration is the


DOI: 10.1021/acsami.9b05383
ACS Appl. Mater. Interfaces XXXX, XXX, XXX−XXX

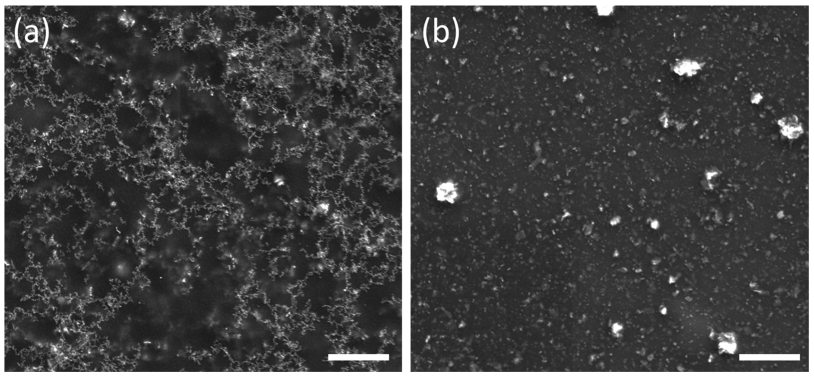


**Figure 2.** SEM micrographs of the aggregation patterns formed by the ZnO nanoparticles with binder polymers: (a) HEC and (b) HES. Scale bar is 5 $\mu$m.

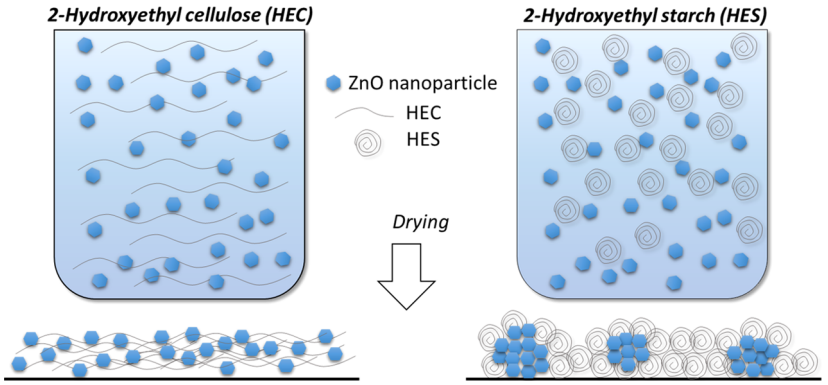


**Figure 3.** Assembly structures of ZnO nanoparticles with HEC (modified cellulose) and HES (modified starch) before and after drying into a nanocomposite. Schematic is not drawn to scale.

depletion force, which depends on many different factors including the polymer dimension and nanoparticle size.[39] It is known that larger polymer dimensions may induce strong and long-range depletion attractions among nanoparticles.[40] In this scenario, HEC again may trigger stronger attractions at a greater distance between ZnO nanoparticles. The strength of this interaction may induce the diffusion-limited aggregation, and the particles can form branched fractal assembly structures. On the other hand, the reduced dimensionality of HES may not induce strong attractions among nanoparticles and form fractal network structures.

We believe that the ZnO nanoparticle aggregation holds the key in differentiating the UV-blocking capabilities of the coating films. Based on our understanding of the system, schematic plots of HEC and HES conformations in aqueous solutions together with the ZnO nanoparticles, as depicted in Figure 3. It further demonstrates the possible assembly structures when the coatings are dried. When HES is used as the binder, the polymer coils initiate the formation of dense aggregates composed of many particles. Therefore, the contact of UV light with the nanoparticle surface is significantly limited since the aggregation drastically reduces the exposed ZnO surface area. In comparison, the loose fractal clusters formed under HEC are extended particle by particle, exposing large amounts of nanoparticle surface for interacting with UV radiation. At the same time, the HEC composite is largely transparent, also due to the open fractal structures. To understand the detailed interactions and mechanisms within these systems, more thorough experimental and computational studies are required, which is out of the scope of this paper.

To gain a deeper understanding of the cluster formation and average aggregate size in the coating films, small-angle X-ray scattering (SAXS) measurements were conducted. First, ZnO nanoparticle size is estimated to be 14.9 nm based on SAXS fitting result of the HES sample, which is consistent with the electron microscope measurement (Figure S1). We adopted a model that is derived from a fractal system with polydispersed primary particles to calculate the scattering intensity (eqs S1–S4).[41−43] The quality of the model fitting is calculated according to eq S5. The model grants insight into the quantitative characterization of aggregates including the Guinier radius of the fractal, correlation length, fractal dimension, and the corresponding aggregation number, denoted as the number of primary particles incorporated in a single fractal cluster. The fitted and experimental curves are plotted in Figure 4. The shoulder from high $q$ region corresponds to ZnO primary particles, whereas the shoulder presented in low $q$ region is directly related to fractal clusters. The two-level structures observed in both 1.3 M and 90k HEC demonstrate the dimension of fractal clusters by the existence of another Guinier region at low $q$. This confirms the fractal structures at the micron scale observed in SEM micrographs. In HES, a one-level structure is present, with no evidence of the shoulder at low $q$. This suggests that HES does not form fractal aggregates in a SAXS detectable length scale. The values for correlation length, aggregation number, and Guinier radius of fractal clusters are listed in Table 2. It is shown that a higher value of correlation length, Guinier radius (eq S6), and a significantly larger value for the aggregation number (eq S7) are observed with HES compared with HEC. The aggregation


DOI: 10.1021/acsami.9b05383
ACS Appl. Mater. Interfaces XXXX, XXX, XXX−XXX

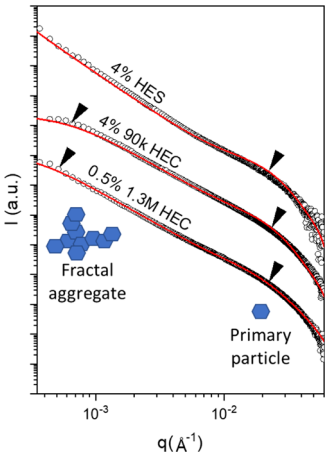


**Figure 4.** Fitted (red) and experimental (black) curves of polymeric binders with commercial ZnO dispersions, with arrows indicating the shoulder regions for the primary particles and fractal aggregates. The larger slope in HES yields a larger radius and a significantly higher aggregation number. Insets show the schematic plot of particle arrangements.

**Table 2. Comparison of Guinier radius and Correlation Length of Clusters and Aggregation Number for Nanocomposite Formulated with HES and HEC**

| sample | correlation length [nm] | Guinier radius [nm] | aggregation number |
|---|---|---|---|
| 4% HES | 1286 | 2945 | 7 481 716 |
| 4% 90k HEC | 152 | 307 | 4110 |
| 0.5% 1.3 M HEC | 292 | 588 | 19 259 |

number for HES is 3 orders of magnitude higher, suggesting that nanoparticles form much bigger and denser aggregates in HES. The large numbers may also indicate that it is inappropriate to use the fractal model in describing ZnO particles, consistent with the morphology in HES binder, as observed in SEM. On the other hand, coating films formulated with HEC of different molecular weights have nearly the same fractal dimension, suggesting that the morphologies evolved through the same mechanistic process. The Guinier radius, correlation length, and aggregation number are correlated to the HEC molecular weight, supporting the idea that the rodlike HEC chains are directly influencing the self-assembly of the nanoparticles. The equations used for the fitting model and calculation of aggregation number, correlation length, fractal dimension, and Guinier radius are explained in detail in the Supporting Information.

Additional verification of the composite effectiveness with HEC as the polymeric binder can be observed in Figure 5a with UV-blocking efficiency at different levels of ZnO loading. In the UV region, the linear trend of absorption in both HEC and HES suggests that as ZnO loading increases, no significance change is observed for UV-blocking efficiency. However, the slope of HEC is greater, suggesting an enhanced efficiency when compared to HES. This result signifies that the fractal structures formed under HEC can maintain the UV-blocking effectiveness throughout a large range of nanoparticle concentration. This data demonstrates the significance and superior performance offered by the fractal assembly structures, since higher nanoparticle concentration oftentimes will lead to more severe aggregation and lower the light blocking efficiency. In the visible region (Figure 5b), HES shows a linear trend. However, HEC shows saturation at ~0.4% ZnO loading. These trends clearly suggest that the fractal network structures formed in HEC are superior in blocking UV while maintaining the transparency at different ZnO concentrations.

**Chemical Dispersant.** Chemical dispersants were also added in the coating formulation to aid the nanoparticle dispersion. It has been observed that a different chemical dispersant is needed to optimize the performance for different types of nanoparticles. For example, sodium polyphosphate promoted the formation of similar dispersion patterns of various nanopowders including ZnO and $TiO_2$ (Figures S6–S8). Under the influence of 90k g/mol HEC (Figure S6), the $TiO_2$ nanopowder, ZnO nanopowder, and ZnO dispersion all show the formation of branch-like fractal structures. With the substitution of the 1.3 M g/mol of HEC counterpart, it is apparent that similarities exist across the different nanoparticle types (Figure S7), though the fractal structures appear more condensed. This is due to the reduced HEC loading, which yields a much thinner, more concentrated composite. Interestingly, the ZnO dispersion (Figure S7b) appears to form most of the assembly beneath the surface of the film, possibly due to the hydrophilic surface modification on the nanoparticles. Correspondingly, the HES coating formulation shows similar aggregation structures among various nanoparticles, all demonstrating the formation of discrete clusters (Figure S8). No fractal network structures were observed in the HES binder. The similar assembly patterns of different nanoparticles in the same binder suggest that the underlying mechanism of assembly may not be specific to the surface

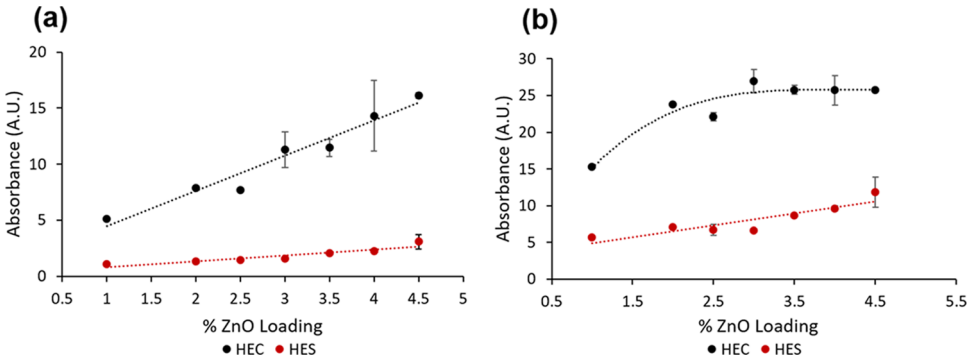


**Figure 5.** UV−vis spectra of HEC and HES binders with ZnO loading in the (a) UVA (354 nm) and (b) visible spectrum (600 nm).


DOI: 10.1021/acsami.9b05383
ACS Appl. Mater. Interfaces XXXX, XXX, XXX−XXX

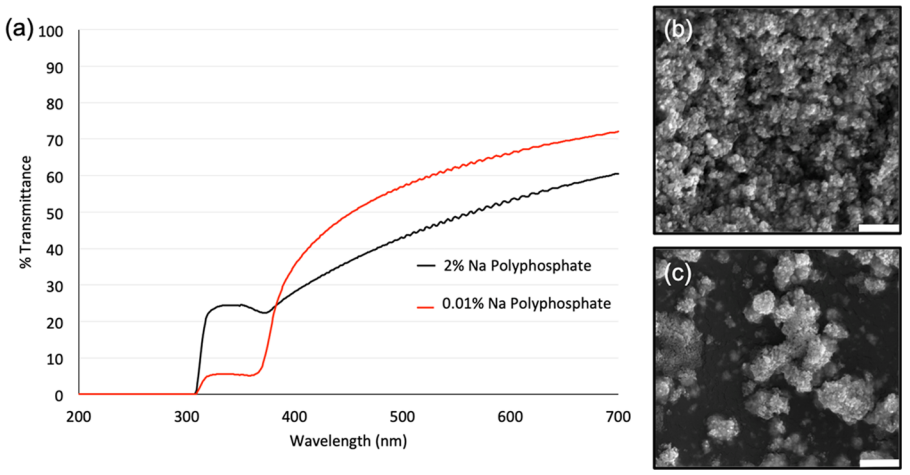


**Figure 6.** (a) UV−vis spectrum of varying concentrations of Na polyphosphate with 0.8% ZnO nanopowders; (b) SEM micrograph of 0.01% Na polyphosphate; (c) SEM micrograph of 2% Na polyphosphate. Scale bar is 1 $\mu$m.

chemistry of nanoparticles. It is also found that the coating capabilities are not determined by the substrate, and switch from PET to poly(vinyl chloride) (PVC) mostly maintains the UV-blocking and transparency (Figure S9). Therefore, the driving factor in the determination of assembly structures is the binder morphology. With the addition of small amounts of sodium polyphosphate (0.01 wt %), similar UV-blocking and transparency performance was achieved with commercial ZnO nanopowders and commercial ZnO nanoparticle dispersions. However, when sodium polyphosphate concentration is increased to a certain threshold (2 wt %), SEM micrographs show the formation of large aggregates, diminishing the UV-blocking capabilities and regularity of the nanocomposite (Figure 6). The aggregation may be due to the increase of the ionic strength in the solution that screens the electrostatic repulsion of the nanoparticles. These results further confirm that nanoparticle assembly structures directly influence the optical properties. More dispersed ZnO nanoparticles and open fractal network structures will produce coating films with better UV-blocking performance and high transparency.

## CONCLUSIONS

A biobased, transparent UV-blocking coating with unique ZnO nanoparticle self-assembly structures was formulated. In this study, two widely used biobased polymers, HEC and HES, were chosen as the coating matrix. Their similarity in composition offers an opportunity to single out the influence of conformational differences on the assembly structures. Future studies will include more binder polymers, which may help reveal more details of the underlying mechanism of nanoparticle assembly. With HEC binders, branch-like fractal network structures were self-assembled. In contrast, large and dense globules of particles were formed with HES. The striking differentiation between the performance of HEC and HES formulations reveals that fundamental self-assembly structures induced by binder polymers can lead to drastically different performances of ZnO nanoparticles. Though ZnO nanoparticles have the inherent ability to absorb UV light, it was found that the open fractal assembly networks are essential to achieve transparency and high UV-blocking efficacy. This capability has been shown across a variety of substrates including poly(ethylene terephthalate) (PET) and poly(vinyl chloride) (PVC). The overall thickness of the composite ranges from 0.2 to 2.5 $\mu$m, which is significantly thinner than the previously reported technologies. This simple and straightforward formulation provides a cost-effective and readily scalable solution to the continual issue of UV degradation. The thin thickness, high UV-blocking, and transparency of the nanocomposite grant its applicability in a variety of fields, such as food packaging and cosmetics. In addition, this work can be extended to a platform of biobased coating technology, which creates dispersed nanoparticles of highly fractal assembly patterns. The coating film properties, such as scratch resistance, adhesion, and water resistance, can be further improved by crosslinking or adding a top coat. It is also possible to directly reverse print the thin coating film on the plastic substrate for food packaging applications.

## EXPERIMENTAL SECTION

**Coating Formulation.** All of the chemicals used in this study are commercially available, and the sources are listed in the Supporting Information. In a glass vial, modified starch/cellulose (1.2 g) was diluted to 4 wt %. The mixture was stirred at 550 rpm for 2 min, modified with ammonia hydrodroxide (to pH 9), and stirred once more for 5 min. The solution was then heated under microwave irradiation. Following, a separate mixture of ZnO nanoparticles (0.24 g), Na polyphosphate (0.006 g), and deionized water (0.95 mL) was stirred and sonicated for 5 min. The solution was diluted with deionized water (3 mL), stirred 5 additional min, and then homogenized for 5 min. A commercial ZnO nanoparticle dispersion can replace the previous, with Tween 20 (0.075 g) as the dispersant and an additional 20 min of sonication in place of the homogenization step. The binder solution and nanoparticle dispersions were combined at 550 rpm for 10 min. In the case of the nanopowder dispersion, the mixture was homogenized for 5 min, whereas with the commercial dispersion, the mixture was sonicated for 20 min. After thorough homogeneity has been achieved, the formulation was drawn down on corona-treated polyethylene plastic with a stainless steel drawdown bar of 75 $\mu$m wet thickness.

**Materials Characterization.** A Tecnai F20 microscope operating at 200 kV was used to acquire bright-field transmission electron microscopy images. Scanning electron microscope micrographs were taken via a field-emission scanning electron microscope (Nanonova 230, FEI). The UV-blocking capability and transparency were assessed via the use of a UV−vis spectrometer (Cary 5000-Vis-NIR, Agilent). Laser light diffraction was measured with a dynamic light scattering (Zetasizer NanoZS, Malvern). X-ray diffraction studies were taken on a small-angle X-ray scattering diffractometer (Xeuss 2.0


DOI: 10.1021/acsami.9b05383
ACS Appl. Mater. Interfaces XXXX, XXX, XXX−XXX

SWAXS, XENOCS, France), with analysis conducted using the SASView computational software.

## ■ ASSOCIATED CONTENT

### Supporting Information

The Supporting Information is available free of charge on the ACS Publications website at DOI: 10.1021/acsami.9b05383.

Experimental chemicals and instrumentation (SEM, UV−vis spectroscopy, confocal microscopy, dynamic light scattering, small-angle X-ray scattering); small-angle X-ray scattering calculations and theory; TEM images of ZnO nanoparticle morphology; UV−vis spectra of $TiO_2$ coatings with various polymeric binders; confocal micrographs of the HEC coating film; and comparative SEM images of different nanoparticles (ZnO nanopowder, ZnO dispersion, and $TiO_2$ nanopowder) under the same binder condition (PDF)

## ■ AUTHOR INFORMATION


### Corresponding Author

*E-mail: sjiang1@iastate.edu.

### ORCID

Fang-Yi Lin: 0000-0002-7235-2596

Eric Cochran: 0000-0003-3931-9169

Shan Jiang: 0000-0001-8119-9012


### Notes

The authors declare no competing financial interest.

## ■ ACKNOWLEDGMENTS

S.J. would like to thank Iowa State University for the Start-up Fund and 3 M for the Non-tenured Faculty Award. S.J. would also like to thank Siegwerk USA Inc. for the assistance and advice. This work is partially supported by NSF I/UCRC The Center for Bioplastics and Biocomposites ($CB^2$), Polymer and Food Protection Consortium, American Chemical Society Petroleum Research Fund under Grant No. 60264-DNI7 and the Agriculture and Food Research Initiative Grant No. 2019-67013-29016 from the USDA National Institute of Food and Agriculture. The authors also acknowledge NSF-DMR-1626315 for the availability of the small-angle X-ray scattering system.

## ■ REFERENCES


(1) Sambandan, D. R.; Ratner, D. Sunscreens: An Overview and Update. *J. Am. Acad. Dermatol.* **2011**, *64*, 748−758.

(2) Zhao, H.; Li, R. K. Y. A Study on the Photo-Degradation of Zinc Oxide (ZnO) Filled Polypropylene Nanocomposites. *Polymer* **2006**, *47*, 3207−3217.

(3) Andersen, M.; Skibsted, L. *Chemical Deterioration and Physical Instability of Food and Beverages*; CRC Press: Boca Raton, 2010.

(4) Andersen, H. J.; Bertelsen, G.; Boegh-Soerensen, L.; Shek, C. K.; Skibsted, L. H. Effect of Light and Packaging Conditions on the Colour Stability of Sliced Ham. *Meat Sci.* **1988**, *22*, 283−292.

(5) Koutchma, T.; Popović, V.; Ros-Polski, V.; Popielarz, A. Effects of Ultraviolet Light and High-Pressure Processing on Quality and Health-Related Constituents of Fresh Juice Products. *Compr. Rev. Food Sci. Food Saf.* **2016**, *15*, 844−867.

(6) Riaz, M. N.; Rokey, G. J. *Extrusion Problems Solved: Food, Pet Food and Feed*; Woodhead Publishing: Cambridge, 2014.

(7) Wang, Y.; Su, J.; Li, T.; Ma, P.; Bai, H.; Xie, Y.; Chen, M.; Dong, W. A Novel UV-Shielding and Transparent Polymer Film: When Bioinspired Dopamine-Melanin Hollow Nanoparticles Join Polymers. *ACS Appl. Mater. Interfaces* **2017**, *9*, 36281−36829.

(8) Gharibshahi, E.; Saion, E. Influence of Dose on Particle Size and Optical Properties of Colloidal Platinum Nanoparticles. *Int. J. Mol. Sci.* **2012**, *13*, 14723−14741.

(9) Gao, T.; Li, Q.; Wang, T. Sonochemical Synthesis, Optical Properties, and Electrical Properteis of Core/Shell-Type ZnO Nanorod/CdS Nanoparticle Composites. *Chem. Mater.* **2005**, *17*, 887−892.

(10) Kołodziejczak-Radzimska, A.; Jesionowski, T. Zinc Oxide—From Synthesis to Application: A Review. *Materials* **2014**, *7*, 2833−2881.

(11) Chen, X.; Mao, S. S. Titanium Dioxide Nanomaterials: Synthesis, Properties, Modification, and Applications. *Chem. Rev.* **2007**, *107*, 2891−2959.

(12) Cui, H.; Zayat, M.; Parejo, P. G.; Levy, D. Highly Efficient Inorganic Transparent UV-Protective Thin-Film Coating by Low Temperature Sol-Gel Procedure for Application on Heat-Sensitive Substrates. *Adv. Mater.* **2008**, *20*, 65−68.

(13) Ammala, A.; Hill, A. J.; Meakin, P.; Pas, S. J.; Turney, T. W. Degradation Studies of Polyolefins Incorporating Transparent Nanoparticulate Zinc Oxide UV Stabilizers. *J. Nanopart. Res.* **2002**, *4*, 167−174.

(14) Austin, R. Antireflection Layer System with Integral UV Blocking Properties. U.S. Patent US5,332,618A, July 26, 1994.

(15) Fu, F.; Yang, Q.; Zhou, J.; Hu, H.; Jia, B.; Zhang, L. Structure and Properties of Regenerated Cellulose Filaments Prepared from Cellulose Carbamate-NaOH/ZnO Aqueous Solution. *ACS Sustainable Chem. Eng.* **2014**, *2*, 2604−2612.

(16) Hayden, D. R.; Imhof, A.; Velikov, K. P. Biobased Nanoparticles for Broadband UV Protection with Photostabilized UV Filters. *ACS Appl. Mater. Interfaces* **2016**, *8*, 32655−32660.

(17) Li, W.; Li, L.; Cao, Y.; Lan, T.; Chen, H.; Qin, Y. Effects of PLA Film Incorporated with ZnO Nanoparticle on the Quality Attributes of Fresh-Cut Apple. *Nanomaterials* **2017**, *7*, 207−227.

(18) Youssef, A. M.; El-Sayed, S. M. Bionanocomposites Materials for Food Packaging Applications: Concepts and Future Outlook. *Carbohydr. Polym.* **2018**, *193*, 19−27.

(19) Dong, N.; Wang, D.; Yin, Y.; Cai, W.; Qu, F.; Lin, J.; Lu, D.; Han, S. Synthesis of ZnO Sunscreen Composite Using Lamellar Self-Assembly 6-PGME as Template. *Res. Chem. Intermed.* **2019**, *45*, 521−531.

(20) Shi, L.; Jin, L.; Hang, J.; Sun, X. Organic/Inorganic Hybrid Transparent Heat-Insulating Coating Material, and Preparation Method and Application Thereof. China Patent CN103,387,787A, September 28, 2016.

(21) Jiang, S.; Van Dyk, A.; Maurice, A.; Bohling, J.; Fasano, D.; Brownell, S. Design Colloidal Particle Morphology and Self-Assembly for Coating Applications. *Chem. Soc. Rev.* **2017**, *46*, 3792−3807.

(22) Rivero, P. J.; Urrutia, A.; Goicoechea, J.; Arregui, F. J. Nanomaterials for Functional Textiles and Fibers. *Nanoscale Res. Lett.* **2015**, *10*, 501−523.

(23) Derradji, M.; Ramdani, N.; Gong, L.; Wang, J.; Xu, X.; Lin, Z.; Henniche, A.; Liu, W. Mechanical, Thermal, and UV-Shielding Behavior of Silane Surface Modified ZnO-Reinforced Phthalonitrile Nanocomposites. *Polym. Adv. Technol.* **2016**, *27*, 882−888.

(24) Ni, S.; Zhang, H.; Dai, H.; Xiao, H. Starch-Based Flexible Coating for Food Packaging Paper with Exceptional Hydrophobicity and Antimicrobial Activity. *Polymers* **2018**, *10*, 1260−1275.

(25) Hussein, J.; El-Banna, M.; Razik, T. A.; El-Naggar, M. E. Biocompatible Zinc Oxide Nanocrystals Stabilized via Hydroxyethyl Cellulose for Mitigation of Diabetic Complications. *Int. J. Biol. Macromol.* **2018**, *107*, 748−754.

(26) Xiao-Fei, Z.; Xue, L.; Xia, T.; Zhi-Gang, S.; Jian-Feng, C. In *Fabrication of Highly Transparent ZnO/PVB Nanocomposite Films with Novel UV-Shielding Properties*, Presented at the International Nano-electrics Conference, Hong Kong, China, January 3−8, 2010; p 208.

(27) Miklečić, J.; Lučić Blagojević, S.; Petrič, M.; Jirous-Rajkovic, V. Influence of $TiO_2$ and ZnO Nanoparticles on Properties of Waterborne Polyacrylate Coating Exposed to Outdoor Conditions. *Prog. Org. Coat.* **2015**, *89*, 67−74.




DOI: 10.1021/acsami.9b05383
ACS Appl. Mater. Interfaces XXXX, XXX, XXX−XXX

(28) Nguyen, T. V.; Phi Hung, D.; Duong, K.; Duong, Q.; Quoc Trung, V.; Hiep Nguyen, A.; Phuc Mac, V.; Lu Le, T. Effect of R-$TiO_2$ and ZnO Nanoparticles on the UV-Shielding Efficiency of Water-Borne Acrylic Coating. *Prog. Org. Coat.* **2017**, *110*, 114−121.
(29) Babaei-Ghazvini, A.; Shahabi-Ghahfarrokhi, I.; Goudarzi, V. Preparation of UV-Protective Starch/Kefiran/ZnO Nanocomposite as a Packaging Film: Characterization. *Food Packag. Shelf Life* **2018**, *16*, 103−111.
(30) Therias, S.; Larché, J. F.; Bussière, P. O.; Gardette, J. L.; Murariu, M.; Dubois, P. Photochemical Behavior of Polylactide/ZnO Nanocomposite Films. *Biomacromolecules* **2012**, *13*, 3283−3291.
(31) Lowry, M. S.; Hubble, D. R.; Wressell, A. L.; Vratsanos, M. S.; Pepe, F. R.; Hegedus, C. R. Assessment of UV-Permeability in Nano-ZnO Filled Coatings via High Throughput Experimentation. *J. Coat. Technol. Res.* **2008**, *5*, 233−239.
(32) Brown, W.; Henley, D.; Öhman, J. Studies on Cellulose Derivatives. PartII. The Influence of Solvent and Temperature on the Configuration and Hydrodynamic Behavior of Hydroxyethyl Cellulose in Dilute Solution. *Macromol. Chem. Phys.* **1963**, *64*, 49−67.
(33) Banks, W.; Greenwood, C. T. The Conformation of Amylose in Neutral, Aqueous Salt Solution. *Carbohydr. Res.* **1968**, *7*, 349−356.
(34) Wojnarowicz, J.; Chudoba, T.; Gierlotka, S.; Lojkowski, W. Effect of Microwave Radiation Power on the Size of Aggregates of ZnO NPs Prepared Using Microwave Solvothermal Synthesis. *Nanomaterials* **2018**, *8*, 343−360.
(35) Vaishnav, D.; Goyal, R. K. Thermal and Dielectric Properties of High Performance Polymer/ZnO Nanocomposites. *IOP Conf. Ser.: Mater. Sci. Eng.* **2014**, *64*, No. 012016.
(36) Xiong, H.-M.; Zhao, X.; Chen, J.-S. New Polymer—Inorganic Nanocomposites: PEO—ZnO and PEO—ZnO—$LiClO_4$ Films. *J. Phys. Chem. B* **2001**, *105*, 10169−10174.
(37) Jassby, D.; Farner Budarz, J.; Wiesner, M. Impact of Aggregate Size and Structure on the Photocatalytic Properties of $TiO_2$ and ZnO Nanoparticles. *Environ. Sci. Technol.* **2012**, *46*, 6934−6941.
(38) Tokumoto, M. S.; Pulcinelli, S. H.; Santilli, C. V.; Craievich, A. F. Electro-Chemical Deposition of Zinc Oxide Nanostructures by Using Two Electrodes. *J. Non-Cryst. Solids* **1999**, *247*, 176−186.
(39) Ray, D.; Aswal, V. K.; Kohlbrecher, J. Micelle-Induced Depletion Interaction and Resultant Structure in Charged Colloidal Nanoparticle System. *J. Appl. Phys.* **2015**, *117*, 164310−164319.
(40) Lekkerkerker, H.; Tuinier, R. *Colloids and the Depletion Interaction*; Springer: Heidelberg, 2011.
(41) Caetano, B.; Santill, C.; Meneau, F.; Briois, V.; Pulcinelli, S. In Situ and Simultaneous UV-Vis/SAXS and UV-Vis/XAFS Time-Resolved Monitoring of ZnO Quantum Dots Formation and Growth. *J. Phys. Chem. B* **2011**, *115*, 4404−4413.
(42) Baeza, G.; Genix, A.; Degrandcourt, C.; Petitjean, L.; Gummel, J.; Couty, M.; Oberdisse, J. Multiscale Filler Structure in Simplified Industrial Nanocomposite Silica/SBR Systems Studied by SAXS and TEM. *Macromolecules* **2013**, *46*, 317−329.
(43) Teixeira, J. Small-Angle Scattering by Fractal Systems. *J. Appl. Crystallogr.* **1988**, *21*, 781−785.


DOI: 10.1021/acsami.9b05383
*ACS Appl. Mater. Interfaces* XXXX, XXX, XXX−XXX